

Indirect detection of low-mass dark matter through the π^0 and η windows

J. G. Christy,¹ Jason Kumar,¹ and Arvind Rajaraman²

¹*Department of Physics & Astronomy, University of Hawai'i, Honolulu, HI 96822, USA*

²*Department of Physics and Astronomy, University of California, Irvine, CA 92697, USA*

We consider the search for gamma rays produced by the annihilation or decay of low-mass dark matter which couples to quarks. In this scenario, most of the photons are produced from the decays of π^0 or η mesons. These decays produce distinctly different photon signatures due to the difference in meson mass. We assess the ability of the future MeV-range observatories to constrain the hadronic final states produced by dark matter annihilation or decay from the shape of the resulting photon spectrum. We then comment on how this information can be used to determine properties of the dark matter coupling to the quark current, based on the approximate symmetries of low-energy QCD.

I. INTRODUCTION

The annihilation or decay of dark matter to Standard Model particles can have interesting features if the dark matter is relatively light ($m_\chi \lesssim \mathcal{O}(\text{GeV})$), particularly if dark matter couples to quarks (see, for example, [1–11]). Because the dark matter mass is not very much heavier than that of the lightest hadrons, one must consider these processes as interactions between dark matter and mesons. The dominant gamma-ray signature of these processes then arises from the decay of these light mesons.

The main mechanisms by which the lightest pseudoscalar and vector mesons produce photons are the decays $\pi^0, \eta \rightarrow \gamma\gamma$, where the π^0 and η are either produced directly from dark matter annihilation/decay, or as the subsequent decay products of other heavier mesons. Photons are also produced by the decays of the η' and ω , but they are considerably heavier, and not always kinematically accessible for low-energy processes. Because of the low center-of-mass energy of the process, the π^0 and η are typically produced with only moderate boost. As a result, the photon signals from the π^0 and η are relatively easy to distinguish from each other. Our goal in this paper is to study the ability of future MeV-range gamma-ray experiments, such as e-ASTROGAM [12] or AMEGO [13], to distinguish between the possible final states produced by dark matter annihilation/decay, based on the differences in the photon spectral shape arising from the expected numbers of π^0 and η produced per interaction.

These results are of relevance because the relative number of π^0 and η produced in each interaction is controlled by the Lorentz and isospin structure of the interaction. For example, if dark matter couples to light quarks through a vector interaction, then one expects a small amount of η production [6]. On the other hand, if the coupling structure is scalar or pseudoscalar, then a significant fraction of η s can be produced, depending on the isospin structure of the interaction [5]. Thus, determining the meson content of the final states produced by dark matter decay or annihilation can reveal information about the symmetry structure of microscopic dark matter interactions.

It is important to emphasize that these results do not depend on the details or validity of chiral perturbation theory, but rather on the approximate symmetries of quark interactions at energies well below the electroweak scale. If we assume that dark matter interactions with quarks respect C and P , then the final state quantum numbers under J , C , P and isospin will be the same as those of the quark current to which the dark matter couples. At the energies which we consider, there may be large corrections to amplitudes computed using the chiral Lagrangian, but these will not affect our results, which depend only on the final states which are allowed by the symmetries of the low-energy theory.

We will see that, given the energy resolution, angular resolution, and exposure expected from the next generation of MeV-range gamma-ray experiments, one would expect to be able to distinguish final states in which an η is produced. It is much more difficult to distinguish final states in which only pions are produced. Even an increase in exposure by a factor of 10 is not sufficient to clearly distinguish final states which only involve pions. But improvement in the expected energy resolution would allow one to distinguish between final states which only produce pions.

The plan of this paper is as follows. We will discuss the photon spectrum in Sec. II. We will describe our analysis and results in Sec. III. We discuss the implications of these results in Sec. IV. Finally, we conclude in Sec. V.

II. GAMMA-RAY SPECTRUM

We will focus on neutral mesonic final states which contain at most two or three mesons. We expect that, provided at least one such state is kinematically accessible and allowed by the approximate symmetries of the theory, it should dominate over phase space suppressed final states with larger numbers of mesons. Since we are interested in final states which respect the approximate symmetries of QCD, we are only interested in states with vanishing net strangeness.

In Table 1, we list all of the light pseudoscalar and vector mesons, as well as the branching fractions to decay channels which produce non-negligible numbers of photons [14].¹ It is readily seen that none of the mesons which are lighter than the η' has a significant branching fraction to states which contain an η . As a result, the only primary final states for which photons are produced by η decay are $\pi^0\eta$ and $\pi\pi\eta$. For all other states, photons are produced almost entirely from π^0 , where the π^0 is produced either in the primary process or in the cascade decays of heavier mesons.

The photon spectrum produced by isotropic diphoton decay has been discussed in detail in Refs. [6, 15]. Of particular relevance for this work is that, if the parent particle, with mass m , is not heavily boosted, then

¹ Note, we include the π^\pm and ρ^0 for completeness, despite the fact that all of their decay channels with significant branching fraction produce only a small number of photons.

the photon spectrum is relatively tightly peaked at $E_* = m/2$. Indeed, if plotted against $\log E_\gamma$, it can be shown that the photon spectrum has a global maximum at E_* . Since the η is ~ 4 times heavier than the π^0 ($m_{\pi^0} = 135$ MeV, $m_\eta = 548$ MeV), this implies that final states containing an η will yield photon spectra with support at higher energies than those of final states involving only π^0 . This feature will be useful in allowing us to distinguish the photon spectra arising from different final states, based on their differing η content.

Meson	Mass (MeV)	$J^{P(C)}$	Decay mode	BF
π^0	135	$0^{-(+)}$	2γ	98.8%
π^\pm	140	0^-	$\mu^\pm\nu$	100%
K^\pm	494	0^-	$\pi^\pm\pi^0$	20.7%
			$\pi^0 e^\pm\nu$	5%
			$\pi^0\mu^\pm\nu$	3.4%
			$\pi^\pm\pi^0\pi^0$	1.8%
K_S^0	498	0^-	$\pi^0\pi^0$	30.7%
K_L^0	498	0^-	$\pi^0\pi^0\pi^0$	19.5%
			$\pi^+\pi^-\pi^0$	12.5%
η	548	$0^{-(+)}$	2γ	39.4%
			$3\pi^0$	32.7%
			$\pi^+\pi^-\pi^0$	22.9%
ρ^\pm	775	$1^{-(-)}$	$\pi^\pm\pi^0$	100%
ρ^0	775	$1^{-(-)}$	$\pi^+\pi^-$	100%
ω	783	$1^{-(-)}$	$\pi^+\pi^-\pi^0$	89%
			$\pi^0\gamma$	8%
K^{*0}	892	1^-	$K\pi$	100%
$K^{*\pm}$	892	1^-	$K\pi$	100%
η'	958	$0^{-(+)}$	$\pi^+\pi^-\eta$	42.5%
			$\rho^0\gamma$	29.5%
			$\pi^0\pi^0\eta$	22.4%
ϕ	1019	$1^{-(-)}$	K^+K^-	49.2%
			$K_L^0K_S^0$	34%
			$\rho\pi + \pi^+\pi^-\pi^0$	15.2%

TABLE I: The relevant masses, $J^{P(C)}$ quantum numbers, decay modes and branching fractions (BF) for the light pseudoscalar and vector mesons.

To illustrate, we consider four particular final states: $\pi^0\eta$, $\pi\pi\eta$ (with the $\pi\pi$ state having isospin 0), K^+K^- and K_LK_S . We plot the photon energy spectrum (normalized to unity) for the $\pi^0\eta$, $\pi\pi\eta$, K^+K^- and K_LK_S states (with \sqrt{s} (MeV) = 690, 835, 1000, and 1000 respectively), in Fig. 1. As can be seen by eye, the most marked similarities and differences in the spectra are related to the η content of the final state. States with an η produce a narrow peak near $m_\eta/2$ and another narrow peak near $m_\pi/2$, while states with no η s produce a single broader peak near $m_\pi/2$. The width of these features is determined by how boosted the η and π^0 are, in the center-of-mass frame. As a result, these differences will become less significant at larger center-of-mass energies.

III. ANALYSIS AND RESULTS

We consider a mock analysis of data from one dwarf spheroidal galaxy: Draco. We assume that it is observed by an experiment with a nominal exposure of 3000 $\text{cm}^2 \text{ yr}$ and an energy resolution of 30%. These approximately match the energy resolution and exposure expected of e-ASTROGAM, for example, with a couple of years of run time [12]. We assume Draco is observed with an aperture of 1.3° and that the angular resolution is small compared to this size.

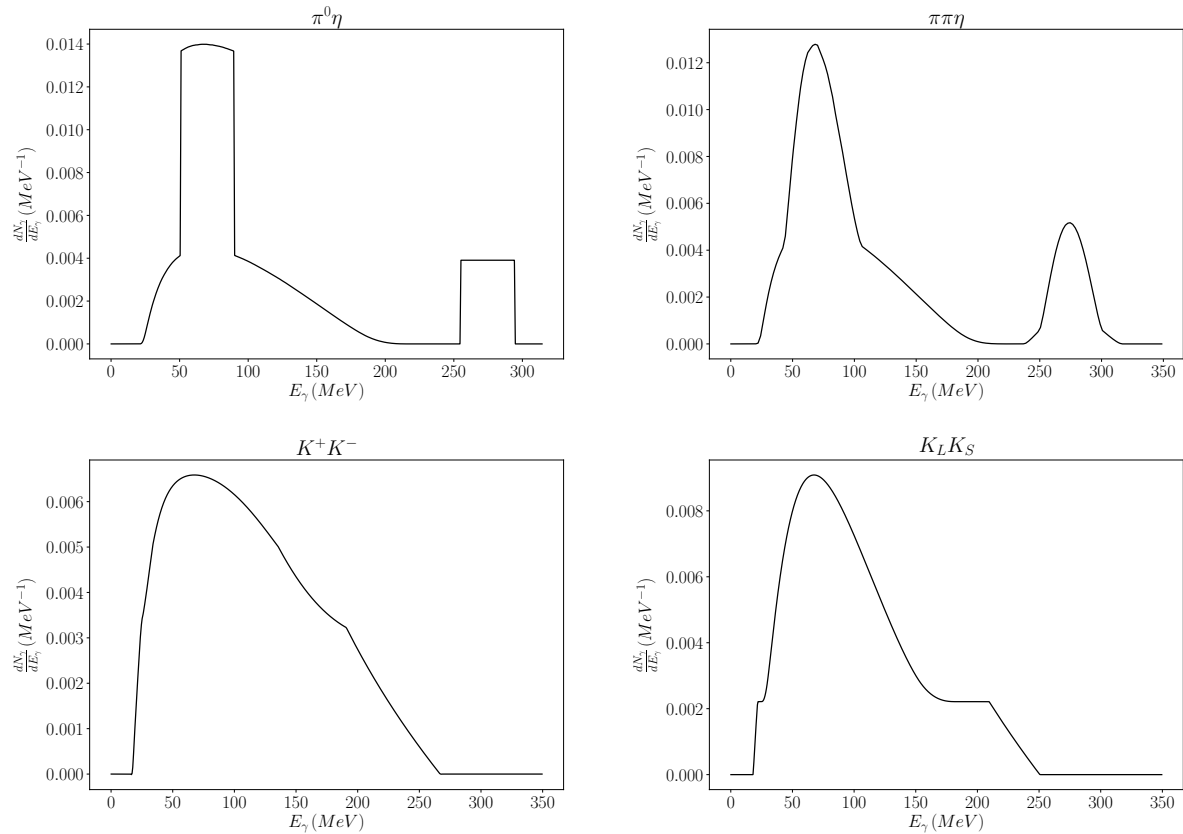


FIG. 1: The gamma ray spectra for considered decay channels near their respective thresholds. The top left panel shows the spectrum for $\pi^0\eta$ with $\sqrt{s} = 690$ MeV. The top right panel shows the spectrum for $\pi\pi\eta$ with $\sqrt{s} = 835$ MeV. The bottom left panel shows the spectrum for K^+K^- with $\sqrt{s} = 1000$ MeV. The bottom right panel shows the spectrum for $K_L K_S$ with $\sqrt{s} = 1000$ MeV. All four spectra have peaks around $m_\pi/2$. This peak is narrower when the decay products include η s; such states also feature a secondary peak near $m_\eta/2$.

For this mock analysis, we assume for simplicity that the signal consists of photons produced by dark matter decay, in order to avoid the tight constraints on low-mass dark matter annihilation which have been obtained from Planck [16, 17].² The differential signal flux can then be expressed as

$$\frac{d^2\Phi_S}{d\Omega dE_\gamma} = \frac{\Gamma}{4\pi m_X} J \frac{dN_\gamma}{dE_\gamma}, \quad (1)$$

where Γ is the decay rate, dN_γ/dE_γ is the photon spectrum, and J is the J -factor. We will use an angle-averaged J -factor for decaying dark matter given by [19]

$$\bar{J}_{dec.} = 5.77 \times 10^{21} \text{ GeV cm}^{-2} \text{ sr}^{-1}. \quad (2)$$

² Note that the bounds from Planck are only stringent if dark matter annihilates from an s -wave state. If dark matter couples to a scalar quark current, as would be the case if the final state were $\pi^0\eta$ [5], then the dark matter annihilation cross section would be p -wave suppressed (see, for example [18]), and the Planck bounds would not be constraining.

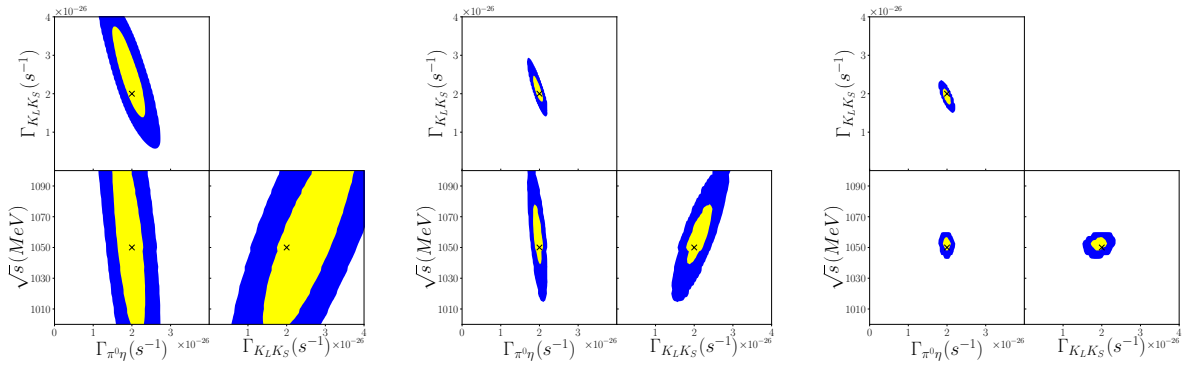


FIG. 2: Projections of three-dimensional 2σ (yellow) and 5σ (blue) confidence level contours onto two-dimensional subspaces, as labeled by the axes, for the $\pi\eta$ and $K_L K_S$ decay channels. The black X represents the model with which the mock data were generated. The left panel shows $3000 \text{ cm}^2 \text{ yr}$ exposure and 30% energy resolution. The middle panel shows $30000 \text{ cm}^2 \text{ yr}$ exposure and 30% energy resolution. The right panel shows $30000 \text{ cm}^2 \text{ yr}$ exposure and 3% energy resolution.

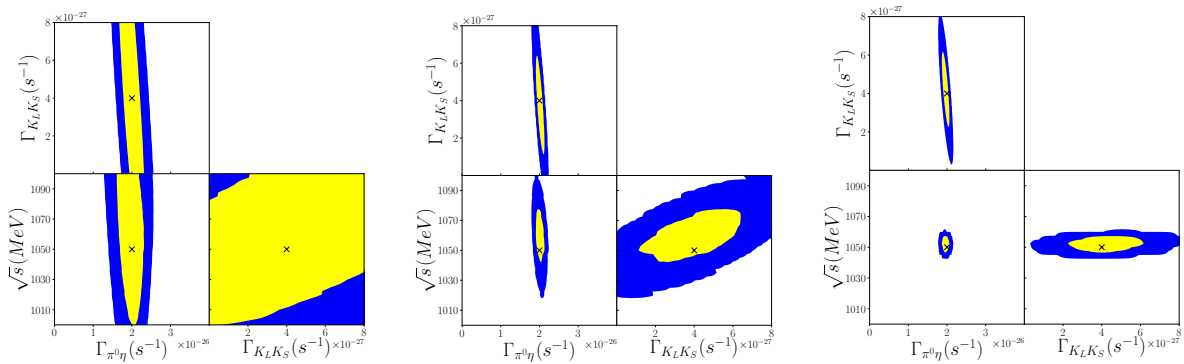


FIG. 3: Similar to Fig. 2, except the true model has $\Gamma_{\pi^0\eta} = 2 \times 10^{-26} \text{ s}^{-1}$, $\Gamma_{K_L K_S} = 4 \times 10^{-27} \text{ s}^{-1}$.

A detailed estimate for the astrophysical foreground and background in this energy range from the direction of Draco is not yet available. When next generation observatories take data, they will be able to estimate the backgrounds by observing slightly off axis from the dSph [20–24]. But for the purpose of our mock data analysis, the only thing we require is an estimate of the background flux, and we can obtain this from data from COMPTEL and EGRET [25]. Their isotropic flux data in the $0.8 - 30 \text{ MeV}$ range can be fit to a power-law form, yielding a differential flux [1]

$$\frac{d^2\Phi_B}{d\Omega dE_\gamma} = 2.74 \times 10^{-3} \left(\frac{E_\gamma}{\text{MeV}} \right)^{-2.0} \text{ cm}^{-2} \text{ s}^{-1} \text{ sr}^{-1} \text{ MeV}^{-1}. \quad (3)$$

Note that a future experiment may discover many more point sources in this energy range, and masking these point sources may yield a considerably smaller flux. In that sense, this estimate may be conservative.

We generate mock data by assuming a particular exposure, and drawing the number of signal and background photons from a Poisson distribution whose mean is given by the expected number of photons

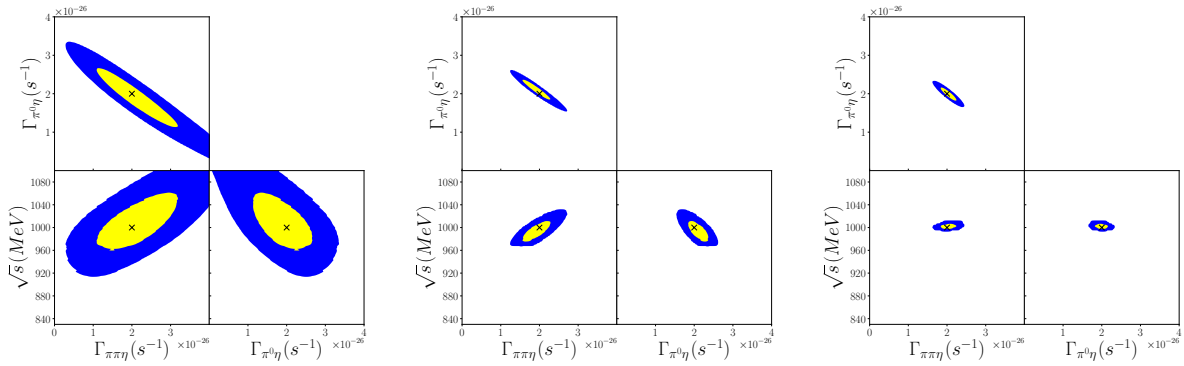


FIG. 4: Projections of three-dimensional 2σ (yellow) and 5σ (blue) confidence level contours onto two-dimensional subspaces, as labeled by the axes, for the $\pi\pi\eta$ and $\pi^0\eta$ decay channels. The black X represents the model with which the mock data was generated. The left panel shows $3000 \text{ cm}^2 \text{ yr}$ exposure and 30% energy resolution. The middle panel shows $30000 \text{ cm}^2 \text{ yr}$ exposure and 30% energy resolution. The right panel shows $30000 \text{ cm}^2 \text{ yr}$ exposure and 3% energy resolution.

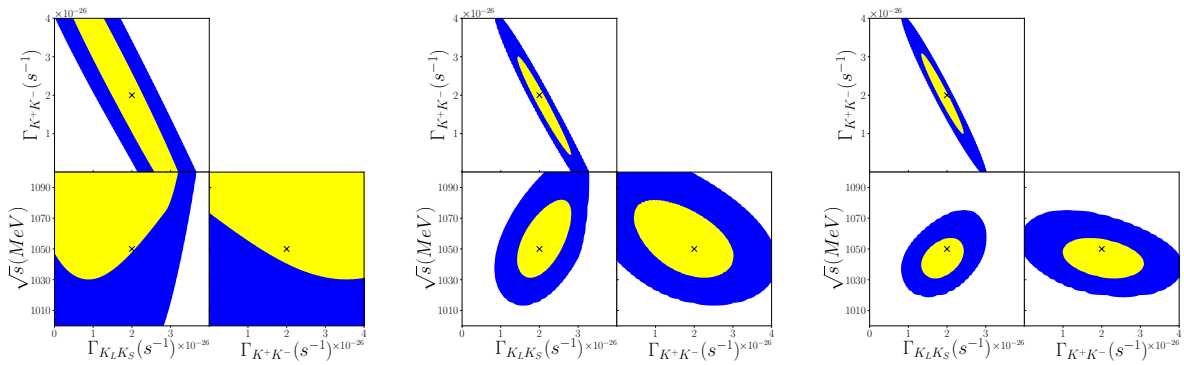


FIG. 5: Projections of three-dimensional 2σ (yellow) and 5σ (blue) confidence level contours onto two-dimensional subspaces, as labeled by the axes, for the $K_L K_S$ and $K^+ K^-$ decay channels. The black X represents the model with which the mock data was generated. The left panel shows $3000 \text{ cm}^2 \text{ yr}$ exposure and 30% energy resolution. The middle panel shows $30000 \text{ cm}^2 \text{ yr}$ exposure and 30% energy resolution. The right panel shows $30000 \text{ cm}^2 \text{ yr}$ exposure and 3% energy resolution.

with true energy in the range $10 \text{ MeV} - 1 \text{ GeV}$. The photons are assigned true energies given by the photon spectrum for either the background (given by Eq. 3) or the signal model (as described in Sec. III). Finally, the measured energies of each photon are drawn from a Gaussian distribution centered at the true energy, with a width determined by the energy resolution. For this analysis, we will assume that dark matter decay can only yield two possible final states. The true model is then defined by three parameters: the dark matter mass, and the partial decay width to each of the two final states.

For this analysis, we will adopt, as conservative choices, an exposure of $3000 \text{ cm}^2 \text{ yr}$, and an energy resolution of 30%. But we will also consider optimistic scenarios in which the exposure is a factor of 10 larger ($30000 \text{ cm}^2 \text{ yr}$). It is also interesting to consider possible improvements in energy resolution for

upcoming experiments. The Advanced Particle-astrophysics Telescope is a proposed experiment which may achieve an energy resolution of $\sim 10\%$ at ~ 100 MeV [26]. Optimistically, we will consider an improvement in the energy resolution to 3% , which is a factor of 10 better than the conservative energy resolution.

We then scan over models, computing the likelihood of the mock data given the model. In computing the likelihood, the combined energy spectrum of signal and background is convolved against the energy resolution function. We can then identify the parameter point of maximum likelihood, along with 2σ and 5σ parameter confidence level surfaces. Figures 2-5 show these confidence level surfaces in our three-dimensional parameter space projected onto three two-dimensional subspaces.

We first consider a scenario in which the true model is dark matter with a mass $m_X = 1050$ MeV, decaying to $\pi^0\eta$ ($\Gamma_{\pi^0\eta} = 2 \times 10^{-26}$ s $^{-1}$) and $K_L K_S$ ($\Gamma_{K_L K_S} = 2 \times 10^{-26}$ s $^{-1}$). This scenario is easily allowed by constraints from Planck [16], which constrains the injection of energy near the time of recombination, but which yields bounds which are 2 orders of magnitude weaker. In Fig. 2, we plot 2D projections of the 2σ (blue) and 5σ (yellow) constraint ellipsoids (the true model is denoted by a black X). In the left panel, we adopt conservative exposure and energy resolutions of 3000 cm 2 yr and 30% , respectively. In the middle panel, we assume an exposure 10 times larger, with a conservative energy resolution. In the right panel, we assume an exposure 10 times larger with an energy resolution 10 times better (3%). We see that even with our conservative exposure and energy resolution, one can find strong evidence for dark matter decay. Moreover, with the conservative exposure one can also determine that both the $\pi^0\eta$ and $K_L K_S$ are present. That is, the hypothesis that either channel has vanishing partial decay width can be rejected at 5σ C.L. If we assume that the branching fractions to the $\pi^0\eta$ and $K_L K_S$ final states are each 50% (with $\sqrt{s} = 1050$ MeV), then 5σ discovery of dark matter decay can be made for a total decay rate as low as $\Gamma = 5 \times 10^{-27}$ s $^{-1}$, assuming the conservative exposure and energy resolution (comparable to the results of [5]).

Note, however, that because π^0 is much lighter than kaons, the available phase space for the $K_L K_S$ final state is only about $\sim 20\%$ of that available to the $\pi^0\eta$ final state. One might naturally expect the branching fraction to the $K_L K_S$ final state to be suppressed, making it more difficult to determine if this final state is present at all. To assess this issue, we repeat the analysis above, but for the case in which the true model has $\Gamma_{\pi^0\eta} = 2 \times 10^{-26}$ s $^{-1}$ $\Gamma_{K_L K_S} = 4 \times 10^{-27}$ s $^{-1}$. These results are plotted in Fig. 3. With a conservative choice of exposure and energy resolution, although one can easily detect the presence of the $\pi^0\eta$ channel, one cannot detect the presence of the $K_L K_S$ channel. This is not surprising, as in the absence of the $\pi^0\eta$ channel, the decay rate to $K_L K_S$ alone would be so small one would not have a discovery-level detection of dark matter decay at all. But with increased exposure, we see that one can detect the presence of the $K_L K_S$ at close to the 5σ -level.

We next consider a true model in which the dark matter ($m_X = 1000$ MeV) decays to the $\pi^0\eta$ and $\pi\pi\eta$ states, each with partial decay width of $\Gamma = 2 \times 10^{-26}$ s $^{-1}$. In Fig. 4, we again plot parameter constraints on

this scenario, assuming conservative exposure and energy resolution (left panel), increased exposure (middle panel), or increased exposure and improved energy resolution (right panel). In this case, we again see that the conservative exposure and energy resolution is not only easily sufficient to discover the presence of dark matter decay, but also determine the presence of both the $\pi^0\eta$ and $\pi\pi\eta$ channels. But as with the previous case, we find that more optimistic choices for the exposure and energy resolution greatly improve parameter constraints.

Finally, we consider a true model in which dark matter ($m_X = 1050$ MeV) decays to $K_L K_S$ and $K^+ K^-$, each with partial decay width $\Gamma = 2 \times 10^{-26}$ s $^{-1}$. Neither of these final states produce η s through subsequent decays. In Fig. 5 we again plot parameter constraints on this scenario, assuming conservative exposure and energy resolution (left panel), increased exposure (middle panel), or increased exposure and improved energy resolution (right panel). In this case, although the conservative choices of exposure and energy resolution are sufficient to detect a dark matter annihilation signal at 5σ CL, the presence of the $K^+ K^-$ channel cannot be detected at the 5σ level even with an exposure 10 times larger. However, if the energy resolution is additionally improved to 3%, then the presence of both channels can be determined with nearly 5σ confidence.

The overarching result is that, with a 30% energy resolution and an exposure of 3000 cm 2 yr, one can easily distinguish models which contain η s in the final state (with decay rates which are currently allowed and an $\mathcal{O}(1)$ branching fraction) from models which do not and even discriminate between different final states which contain η s. But an additional improvement by a factor of 10 in both the exposure and the energy resolution would be needed to allow one to distinguish between different final states, neither of which produced η s in subsequent decays.

A. Generalizations

We have thus far considered a somewhat simple analysis, with only four final states, as a proof of principle. We now consider if these result are expected to remain robust if we consider a more detailed analysis.

For example, we have limited ourselves to final states with at most three mesons. Although, for $\sqrt{s} \lesssim$ GeV, one cannot have more than three non-pion mesons, one can potentially have several pions. One expects these multi-pion states to be phase space suppressed and, thus, subdominant. But in any case, the addition of extra pions will not affect the conclusion that one can readily distinguish final states containing η s from those without. Indeed, the main affect of adding extra pions is to reduce the kinetic energy of all mesons, sharpening the features in the photon spectrum around $m_\pi/2$ and $m_\eta/2$.

Since we have focused on the low-energy regime, we have also been able to assume that the only appreciable source of photons is from the diphoton decays of π^0 and η . Photons also arise from the decay $\omega \rightarrow \pi^0\gamma$,

but this decay only has an 8% branching fraction. However, at higher energies, other processes can produce photons. For example, if the η' can be produced, then the decay $\eta' \rightarrow \rho^0 \gamma$ will occur with a 30% branching fraction ($\eta' \rightarrow \gamma \gamma$ will also occur, but with only a 2.3% branching fraction). The decay $\eta' \rightarrow \rho^0 \gamma$ will produce a feature in the photon spectrum at ~ 165 MeV, between the features created by diphoton π^0 decay and η decay. However, as long as the center-of-mass energy is not too large (so the η' is not heavily boosted), this feature should be narrow and readily distinguishable from the feature at $m_\eta/2$ generated by diphoton η decay.

IV. DISCUSSION

Thus far, we have focused on our ability to distinguish the mesonic final states arising from low-mass dark matter decay using upcoming MeV-range gamma-ray data. We now address how one can use this information to learn about the microphysics of dark matter coupling quarks.

For this purpose we utilize the low-energy (approximate) symmetries of QCD. In particular, the mesonic final state will have the same J , P , C and isospin quantum numbers as the quark current to which dark matter couples. Processes violating these selection rules will be suppressed by factors of α_{em} , sG_F , or $(m_u - m_d)^2/s$, and are expected to be small. Thus, a determination of the final states which are produced by dark matter decay or annihilation can reveal the nature of the dark matter-quark coupling.

For example, the $\pi^0 \eta$ state is a component of an isospin triplet, is necessarily even under charge conjugation, and transforms under parity as $(-1)^L$, where L is the orbital angular momentum. Thus, the quantum numbers of this state must be $J^{PC} = 0^{++}$ or 1^{-+} . If it is determined that dark matter decays to $\pi^0 \eta$ with a nonzero partial decay width, then we would know that dark matter couples to a component of an isospin-triplet quark current with the allowed quantum numbers. Only the quark scalar current ($J^{PC} = 0^{++}$) satisfies this constraint, so the observation of a $\pi^0 \eta$ final state would imply that dark matter must couple to an $I = 1$ scalar quark current, where I is the isospin.

By a similar analysis, we can consider the $\pi \pi \eta$ state. The $\pi \pi$ state transforms as $(-1)^{L_\pi}$ under both C and P , where L_π is the orbital angular momentum of the $\pi \pi$ system. Moreover, symmetry of the $\pi \pi$ wave function requires $I = L_\pi \bmod 2$. We thus see that if the $\pi \pi \eta$ state has $J = 0$, then it must be an isospin singlet with quantum numbers $J^{PC} = 0^{-+}$. This implies that the dark matter couples to an $I = 0$ pseudoscalar quark current.

We thus see that, if gamma-ray telescopes provide evidence that dark matter decay produces both $\pi^0 \eta$ and $\eta(\pi \pi)_{I=0}$ final states, one could conclude that the dark matter particle was spin-0, had quark couplings which violated CP , and coupled to a quark current which is not an eigenstate of isospin.

But if dark matter couples to scalar quark currents, and has sufficiently large mass, then one generically

expects the final states K^+K^- and $K^0\bar{K}^0$ to be produced. Expressed in terms of mass eigenstates, the $K^0\bar{K}^0$ state is a linear combination of K_LK_L and K_SK_S , and has a photon spectrum which is the same as K_LK_S . Thus, the presence of final states both with η s and also with only kaons would be evidence that dark matter was spin 0.

On the other hand, if dark matter is spin 1, then its decays cannot produce the $\pi^0\eta$ state, although states such as K^+K^- and K_LK_S are allowed. If one found evidence of final states from dark matter decay containing kaons, but not of $\pi^0\eta$, that would suggest that the dark matter was spin 1 or at least did not couple to an $I = 1$ scalar quark current.

V. CONCLUSION

We have considered the prospects for upcoming MeV-range gamma-ray observatories to distinguish between the hadronic final states which may be produced by the annihilation or decay of dark matter with $\sqrt{s} \lesssim \mathcal{O}(\text{GeV})$. This study is motivated by the fact that, for low-mass dark matter which couples to quarks, the possible hadronic final states are limited by kinematics and by the approximate symmetries of QCD, including angular momentum, C , P , and isospin. The determination of which final states arise from dark matter decay or annihilation can thus provide information about dark matter microphysics.

For the low-mass dark matter which couples to quarks, the dominant mechanism for creating gamma rays is the production of π^0 or η , which decay to $\gamma\gamma$. Each of these decays produces a feature in the photon spectrum centered at half of the meson mass. The spectral feature at $m_\eta/2$ provides the most statistical leverage, since it is typically narrower, and competes against a smaller astrophysical background.

As a result, even with a 30% energy resolution (as is expected from proposed experiments such as AMEGO and e-ASTROGAM), an upcoming experiment observing the Draco dSph with an exposure of $3000 \text{ cm}^2 \text{ yr}$ would likely be able to detect the presence of η s, and to distinguish between two possible final states containing η s.

But if there are no η s in the final state, then it would be difficult, even with larger exposure, to distinguish if the final state is, for example, K_LK_S , as opposed to K^+K^- . But an improvement of the energy resolution by a factor of 10, in addition to the increased exposure, would allow one to distinguish between these final states.

Acknowledgements

We are grateful to Jason Baretz for collaboration at an early stage of this work, and to Eric J. Baxter for useful discussions. The work of J.K. is supported in part by Department of Energy Grant No. DE-SC0010504. A.R. is supported in part by the United States National Science Foundation under Grant No.

-
- [1] K. K. Boddy and J. Kumar, “Indirect Detection of Dark Matter Using MeV-Range Gamma-Ray Telescopes,” *Phys. Rev. D* **92**, no.2, 023533 (2015) doi:10.1103/PhysRevD.92.023533 [arXiv:1504.04024 [astro-ph.CO]].
- [2] K. K. Boddy and J. Kumar, “Minding the MeV gap: The indirect detection of low mass dark matter,” *AIP Conf. Proc.* **1743**, no.1, 020009 (2016) doi:10.1063/1.4953276 [arXiv:1509.03333 [astro-ph.CO]].
- [3] K. K. Boddy, K. R. Dienes, D. Kim, J. Kumar, J. C. Park and B. Thomas, “Lines and Boxes: Unmasking Dynamical Dark Matter through Correlations in the MeV Gamma-Ray Spectrum,” *Phys. Rev. D* **94**, no.9, 095027 (2016) doi:10.1103/PhysRevD.94.095027 [arXiv:1606.07440 [hep-ph]].
- [4] R. Bartels, D. Gaggero and C. Weniger, “Prospects for indirect dark matter searches with MeV photons,” *JCAP* **05**, 001 (2017) doi:10.1088/1475-7516/2017/05/001 [arXiv:1703.02546 [astro-ph.HE]].
- [5] J. Kumar, “Indirect Detection of Sub-GeV Dark Matter Coupling to Quarks,” *Phys. Rev. D* **98**, no.11, 116009 (2018) doi:10.1103/PhysRevD.98.116009 [arXiv:1808.02579 [hep-ph]].
- [6] D. Berger, A. Rajaraman and J. Kumar, “Dark Matter Through the Quark Vector Current Portal,” *Pramana* **94**, no.1, 133 (2020) doi:10.1007/s12043-020-01995-w [arXiv:1903.10632 [hep-ph]].
- [7] A. Coogan, L. Morrison and S. Profumo, “Hazma: A Python Toolkit for Studying Indirect Detection of Sub-GeV Dark Matter,” *JCAP* **01**, 056 (2020) doi:10.1088/1475-7516/2020/01/056 [arXiv:1907.11846 [hep-ph]].
- [8] A. Coogan, A. Moiseev, L. Morrison and S. Profumo, “Hunting for Dark Matter and New Physics with (a) GECCO,” [arXiv:2101.10370 [astro-ph.HE]].
- [9] A. Coogan, L. Morrison and S. Profumo, “Precision gamma-ray constraints for sub-GeV dark matter models,” *JCAP* **08**, 044 (2021) doi:10.1088/1475-7516/2021/08/044 [arXiv:2104.06168 [hep-ph]].
- [10] P. Reimitz, “MeV astronomy with Herwig?,” [arXiv:2102.00041 [hep-ph]].
- [11] T. Plehn, P. Reimitz, P. Richardson, “Hadronic Footprint of GeV-Mass Dark Matter,” *SciPost Phys.* **8**, 092 (2020) doi:10.21468/SciPostPhys.8.6.092 [arXiv:1911.11147 [hep-ph]].
- [12] A. De Angelis *et al.* [e-ASTROGAM], “Science with e-ASTROGAM: A space mission for MeV–GeV gamma-ray astrophysics,” *JHEAp* **19**, 1-106 (2018) doi:10.1016/j.jheap.2018.07.001 [arXiv:1711.01265 [astro-ph.HE]].
- [13] C. A. Kierans [AMEGO Team], “AMEGO: Exploring the Extreme Multimessenger Universe,” *Proc. SPIE Int. Soc. Opt. Eng.* **11444**, 1144431 (2020) doi:10.1117/12.2562352 [arXiv:2101.03105 [astro-ph.IM]].
- [14] P. A. Zyla *et al.* [Particle Data Group], “Review of Particle Physics,” *PTEP* **2020**, no.8, 083C01 (2020) and 2021 update doi:10.1093/ptep/ptaa104
- [15] K. K. Boddy, K. R. Dienes, D. Kim, J. Kumar, J. C. Park and B. Thomas, “Boxes, Boosts, and Energy Duality: Understanding the Galactic-Center Gamma-Ray Excess through Dynamical Dark Matter,” *Phys. Rev. D* **95**, no.5, 055024 (2017) doi:10.1103/PhysRevD.95.055024 [arXiv:1609.09104 [hep-ph]].
- [16] N. Aghanim *et al.* [Planck], “Planck 2018 results. VI. Cosmological parameters,” *Astron. Astrophys.* **641**, A6 (2020) [erratum: *Astron. Astrophys.* **652**, C4 (2021)] doi:10.1051/0004-6361/201833910 [arXiv:1807.06209 [astro-ph.CO]].
- [17] T. R. Slatyer, “Indirect dark matter signatures in the cosmic dark ages. I. Generalizing the bound on s-wave dark matter annihilation from Planck results,” *Phys. Rev. D* **93**, no.2, 023527 (2016) doi:10.1103/PhysRevD.93.023527 [arXiv:1506.03811 [hep-ph]].
- [18] J. Kumar and D. Marfatia, “Matrix element analyses of dark matter scattering and annihilation,” *Phys. Rev. D* **88**, no.1, 014035 (2013) doi:10.1103/PhysRevD.88.014035 [arXiv:1305.1611 [hep-ph]].
- [19] A. Geringer-Sameth, S. M. Koushiappas and M. Walker, “Dwarf galaxy annihilation and decay emission profiles for dark matter experiments,” *Astrophys. J.* **801**, no.2, 74 (2015) doi:10.1088/0004-637X/801/2/74 [arXiv:1408.0002 [astro-ph.CO]].
- [20] A. Geringer-Sameth and S. M. Koushiappas, “Exclusion of canonical WIMPs by the joint analysis of Milky Way dwarfs with Fermi,” *Phys. Rev. Lett.* **107**, 241303 (2011) doi:10.1103/PhysRevLett.107.241303 [arXiv:1108.2914 [astro-ph.CO]].
- [21] M. N. Mazziotta, F. Loparco, F. de Palma and N. Giglietto, “A model-independent analysis of the Fermi Large Area Telescope gamma-ray data from the Milky Way dwarf galaxies and halo to constrain dark matter scenarios,” *Astropart. Phys.* **37**, 26-39 (2012) doi:10.1016/j.astropartphys.2012.07.005 [arXiv:1203.6731 [astro-ph.IM]].
- [22] A. Geringer-Sameth, S. M. Koushiappas and M. G. Walker, “Comprehensive search for dark matter annihilation in dwarf galaxies,” *Phys. Rev. D* **91**, no.8, 083535 (2015) doi:10.1103/PhysRevD.91.083535 [arXiv:1410.2242 [astro-ph.CO]].
- [23] A. Albert *et al.* [HAWC], “Dark Matter Limits From Dwarf Spheroidal Galaxies with The HAWC Gamma-Ray Observatory,” *Astrophys. J.* **853**, no.2, 154 (2018) doi:10.3847/1538-4357/aaa6d8 [arXiv:1706.01277 [astro-ph.HE]].
- [24] K. K. Boddy, J. Kumar, D. Marfatia and P. Sandick, “Model-independent constraints on dark matter annihilation in dwarf spheroidal galaxies,” *Phys. Rev. D* **97**, no.9, 095031 (2018) doi:10.1103/PhysRevD.97.095031

- [arXiv:1802.03826 [hep-ph]].
- [25] A. W. Strong, I. V. Moskalenko and O. Reimer, “Diffuse galactic continuum gamma rays. A Model compatible with EGRET data and cosmic-ray measurements,” *Astrophys. J.* **613**, 962-976 (2004) doi:10.1086/423193 [arXiv:astro-ph/0406254 [astro-ph]].
- [26] T. Aramaki, M. Boezio, J. Buckley, E. Bulbul, P. von Doetinchem, F. Donato, J. P. Harding, C. Karwin, J. Kumar and R. K. Leane, *et al.* “Snowmass2021 Cosmic Frontier: The landscape of cosmic-ray and high-energy photon probes of particle dark matter,” [arXiv:2203.06894 [hep-ex]].